

UC San Diego

UC San Diego Previously Published Works

Title

Multimodal imaging assessment and histologic correlation of the female rat pelvic floor muscles' anatomy

Permalink

<https://escholarship.org/uc/item/62t9c58m>

Journal

Journal of Anatomy, 234(4)

ISSN

0021-8782

Authors

Sheth, Vipul R
Duran, Pamela
Wong, Jonathan
et al.

Publication Date


2019-04-01

DOI

10.1111/joa.12943

Peer reviewed

Multimodal imaging assessment and histologic correlation of the female rat pelvic floor muscles' anatomy

Vipul R. Sheth,¹ Pamela Duran,² Jonathan Wong,^{1,3} Sameer Shah,⁴ Jiang Du,¹ Karen L. Christman,² Eric Y. Chang^{1,3} and Marianna Alperin⁵ 

¹Department of Radiology, University of California San Diego, La Jolla, CA, USA

²Department of Bioengineering, Sanford Consortium for Regenerative Medicine, University of California San Diego, La Jolla, CA, USA

³Radiology Service, VA San Diego Healthcare System, San Diego, CA, USA

⁴Department of Orthopedic Surgery, University of California San Diego, La Jolla, CA, USA

⁵Division of Female Pelvic Medicine and Reconstructive Surgery, Department of Obstetrics, Gynecology, and Reproductive Sciences, University of California San Diego, La Jolla, CA, USA

Abstract

Pelvic floor disorders negatively impact millions of women worldwide. Although there is a strong epidemiological association with childbirth, the mechanisms leading to the dysfunction of the integral constituents of the female pelvic floor, including pelvic floor skeletal muscles, are not well understood. This is in part due to the constraints associated with directly probing these muscles, which are located deep in the pelvis. Thus, experimental models and non-invasive techniques are essential for advancing knowledge of various phenotypes of pelvic floor muscle injury and pathogenesis of muscle dysfunction, as well as developing minimally invasive approaches for the delivery of novel therapeutics. The most widely used animal model for pelvic floor disorders is the rat. However, the radiological anatomy of rat pelvic floor muscles has not been described. To remedy this gap, the current study provides the first detailed description of the female rat pelvic floor muscles' radiological appearance on MR and ultrasound images, validated by correlation with gross anatomy and histology. We also demonstrate that ultrasound guidance can be used to target rat pelvic floor muscles for possible interventional therapies.

Key words: anatomy; magnetic resonance imaging; pelvic floor muscles; rat; ultrasound.

Introduction

Pelvic floor muscle (PFM) dysfunction is a critical defect in the pathogenesis of pelvic floor disorders, which include pelvic organ prolapse, and urinary and fecal incontinence. Collectively, pelvic floor disorders negatively impact the lives of millions of women worldwide, with close to a quarter of the US female population affected (Wu et al. 2014). Despite dealing with this common debilitating condition since antiquity (Peel, 1949; Porter, 1960), the pathophysiology of the female pelvic floor dysfunction has not been fully elucidated to date.

The primary function of the female pelvic floor is to provide support to the pelvic organs and withstand the forces generated by intra-abdominal pressure, gravity, and inertial forces. The passive response to these applied forces is primarily generated by the connective tissue of the vagina and paravaginal attachments to the bony pelvis, and intramuscular extracellular matrix of the striated PFMs, while the active response is provided by the contractile myofibers and vaginal smooth muscle (Peng et al. 2018). Damage to any component of this complex can result in pelvic floor dysfunction, underscoring the multifactorial etiology of pelvic floor disorders.

Despite the complex pathophysiology, epidemiological studies consistently identify vaginal delivery as the most notable risk factor for pelvic floor disorders related to PFM dysfunction. PFMs, which span the pelvic outlet, include the posteriorly located coccygeus and the levator ani complex, comprised off the iliococcygeus and the two portions of the pubovisceralis muscle – pubococcygeus

Correspondence

Marianna Alperin, Department of Obstetrics, Gynecology, and Reproductive Sciences, University of California San Diego, San Diego 9500 Gilman Drive, MC 0863 La Jolla, CA 92093-0863, USA.
E: malperin@ucsd.edu

Accepted for publication 14 December 2018
Article published online 10 February 2019

and puborectalis (Lukacz et al. 2006; Handa et al. 2011; Memon & Handa, 2013). Unfortunately, knowledge beyond this is limited because, realistically, investigations directly probing PFMs in living women are not feasible due to their location deep within the pelvis. However, animal models serve as an invaluable source to establish systematically the mechanisms underlying pelvic skeletal muscle dysfunction consequent to birth injury and potential treatments to counteract it.

The rat is the most widely used experimental model in pelvic floor disorders research. Through a comparative analysis of the human and rat PFM architecture, the main determinant of *in vivo* muscle function, we have previously validated the rat model with respect to PFMs (Alperin et al. 2014; Stewart et al. 2017). Furthermore, using this model, we have discovered the existence of protective pregnancy-induced adaptations in these muscles (Alperin et al. 2015, 2016). The above is the first step in the continuum of research focused on deciphering what segregates women who do and do not sustain PFM birth trauma (Catanzarite et al. 2018). In addition, the rat has been extensively used as a simulated birth injury model to study the mechanisms of maternal injury and postpartum recovery, and to investigate various treatments that directly target the injured pelvic soft

tissues (Wood et al. 2008; Alperin et al. 2010; Cruz et al. 2012; Feola et al. 2014).

Despite the above, the rat PFM anatomy has not been well-delineated using imaging modalities – computed tomography (CT), magnetic resonance imaging (MRI) and ultrasound. MR and ultrasound are the most commonly used imaging techniques for evaluation of the female pelvis and have the potential for qualitative and quantitative measures of muscle injury and recovery. MRI has better soft tissue contrast and can be used for functional assessment of pelvic floor dysfunction (García del Salto et al. 2014). The benefits of ultrasound include higher spatial resolutions, though for a smaller field of view, and higher temporal resolutions which can be used for real-time image guidance and precise delivery of local therapies. CT provides three-dimensional imaging of the bony structures of the pelvis.

The objective of the current study was to delineate the cross-sectional anatomy of the female rat PFMs through CT, MR, and ultrasound imaging, correlated to the corresponding histological muscle analysis. This work provides a foundation for use of these imaging modalities in future investigations that rely on the rat model to study pelvic floor muscle plasticity under physiological conditions, changes due to muscle injury, and muscle regeneration.

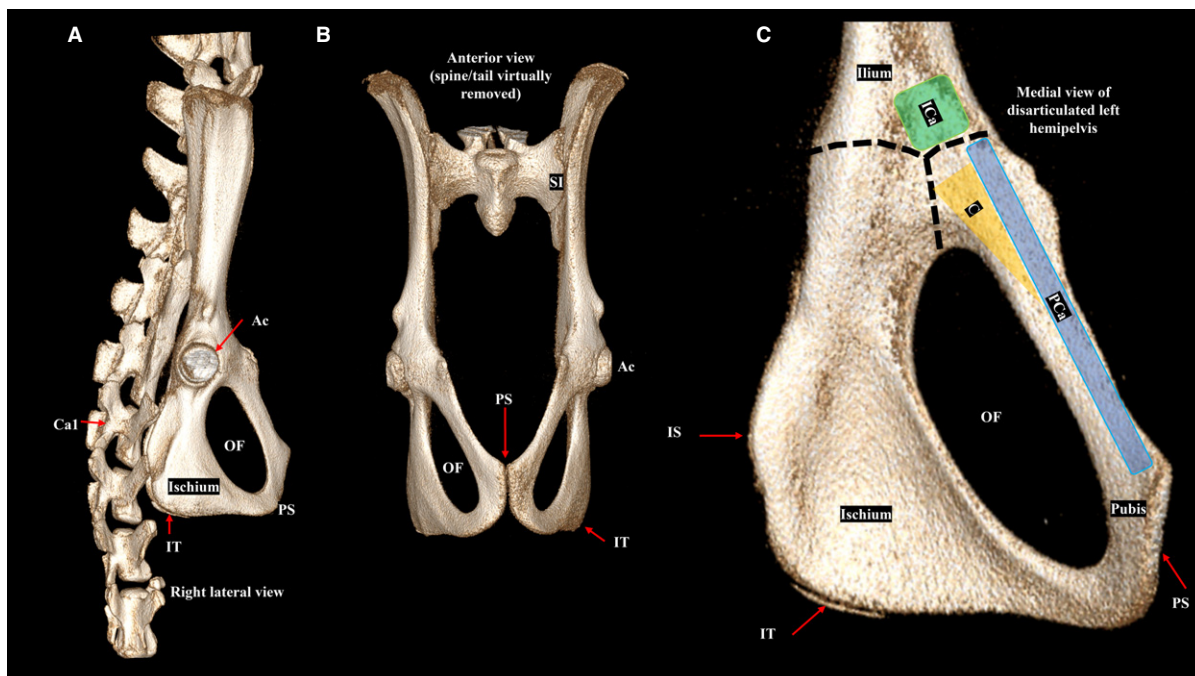


Fig. 1 Volume-rendered computer tomography images of the female rat bony pelvis. (A) Right lateral view of the pelvic bones, sacrum, and proximal caudal vertebra. (B) Anterior view with the spine and tail virtually removed. (C) Medial view of the disarticulated left hemipelvis. The origins of the individual pelvic floor muscles are shown. The dashed lines indicated the physéal scar from the triradiate cartilage. Ac, acetabulum; C, coccygeus (yellow); Ca1, first caudal vertebra; Ica, iliocaudalis (green); IS, ischial spine; IT, ischial tuberosity; OF, obturator foramen; PCa, pubocaudalis (blue); PS, pubic symphysis; SI, sacroiliac joint.

Methods

The University of California, San Diego Institutional Animal Care and Use Committee approved all study procedures. Three-month-old nulligravid female Sprague-Dawley rats ($n = 8$, Envigo, Indianapolis, IN, USA) were used to delineate PFM radiological anatomy. On the day of imaging, animals were euthanized and fur was removed from the lower abdomen and pelvis by chemical depilation (Nair, Church & Dwight, Ewing, NJ, USA). To aid with visualization, the bladder and vagina were distended with 0.5 mL of water-soluble gel (Surgilube, York, PA, USA), using a polyethylene (PE-50) transurethral catheter inserted in a retrograde fashion.

Computed tomography images were acquired on a small animal microCT system using 100 kV, a current of 100 μ A, and 0.009 mm isotropic resolution (Bruker Skyscan 1076, Kontich, Belgium). Volume rendered images were created using RadiAnt DICOM Viewer (Medixant, Poznan, Poland) to better delineate the osseous structures of the pelvis and correlate with results from subsequent MRI and ultrasound. MR imaging was performed on a Bruker 7T/21-cm BioSpec 70/30 ultrasoundR horizontal bore scanner equipped with 72-mm inner diameter quadrature RF volume coil (Bruker Biospin GmbH, Ettlingen, Germany). T2-weighted spin echo images were acquired with chemical shift selective fat saturation, TR 2700 ms, TE 41 ms, 512×512 matrix, 3×5 cm field of view, and 1 mm slice thickness. T1-weighted spin echo images were acquired with chemical shift selective fat saturation, TR 1250 ms, TE 8.6 ms, 512×512 matrix,

3×5 cm field of view and 1 mm slice thickness. MRI included the entire pelvis in the field of view to aid with anatomic delineation and correlation to ultrasound images. Ultrasound was performed on a Vevo MD Imaging System with an ultra-high frequency linear array transducer at 30 MHz center frequency (Fujifilm Visual Sonics, Toronto, ON, Canada). Ultrasound was used to evaluate landmarks for potential image-guided therapies. For illustration of the homology between human and rat PFMs, a T1-weighted MR image with fat saturation from a nulliparous 30-year-old woman is presented. MRI was obtained on a 3T GE MRI, using a LAVA Water sequence, with TR 175 ms, and TE 2.5 ms, 32×32 cm field of view, and 4 mm slice thickness. The T1-weighted image was chosen for better image quality to highlight the human PFMs.

To demonstrate the potential for ultrasound-guided interventions, selected specimens were targeted by image-guided injection of 20 μ L hydrogel labeled with a fluorescent probe, Alexa Fluor 568 (Molecular Probes, Eugene, OR, USA). After imaging, rats ($n = 2$) were rapidly frozen in isopentane cooled with liquid nitrogen to preserve *in vivo* muscle morphology (Meng et al. 2014) and were sectioned using a bandsaw to facilitate histologic processing. Tissues were fixed (Z-Fix, Anatech Ltd, Battle Creek, MI, USA), decalcified, and paraffin-embedded. Blocks were sectioned at 5 μ m and stained with hematoxylin and eosin (H&E) and trichrome stain. In samples with hydrogel injection, tissues were embedded in Optimal Cutting Temperature (OCT), cryosectioned, and imaged with fluorescent microscopy (Leica DM600B with Leica DFC 365FX camera, Leica Microsystems, Wetzlar, Germany).

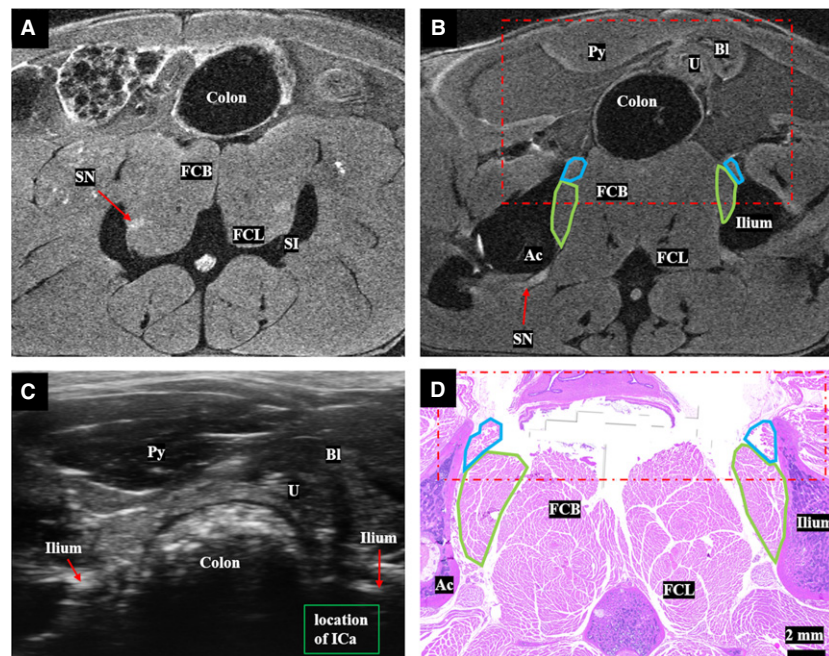


Fig. 2 (A) Sacroiliac level: T2-weighted MR image at the level of the inferior sacroiliac joint, above the level of the pelvic floor muscles. The flexor caudalis brevis and longus muscles, which are important to distinguish from the pelvic floor muscles, are shown immediately medial to the sciatic nerve. (B) Origin of iliocaudalis: T2-weighted magnetic resonance image at the level of the origin of the iliocaudalis (green outline) and superior portion of the pubocaudalis origin (blue outline) shown at the medial inferior surface of the ilium and superior pubic ramus, respectively. The sciatic nerve is visible exiting the pelvis through the sciatic foramen. The red dot/dash box shows the field of view of the ultrasound at the same level. (C) Ultrasound image at the level of the iliocaudalis origin at the medial inferior surface of the ileum. Shadowing from the ilium and stool in the rectum can limit visualization of iliocaudalis. (D) Corresponding histology of the iliocaudalis (green outline) and the pubocaudalis (blue outline). Ac, acetabulum, Bl, bladder, FCB, flexor caudalis brevis, FCL, flexor caudalis longus, ICa, iliocaudalis, PCA, pubocaudalis, Py, pyramidalis muscle, SI, sacroiliac joint, SN, sciatic nerve, U, uterus.

Results

When evaluating cross-sectional images, osseous landmarks provide orientation in the cranial-caudal direction and facilitate identification of the three individual muscles that

comprise the rat PFM complex: the coccygeus, and the two components of the levator ani muscles – pubocaudalis and iliocaudalis. Specifically, the levels of interest are the sacroiliac joints, acetabulum, obturator foramen, and pubic symphysis (Fig. 1A-C). The sacroiliac (SI) joints are an especially

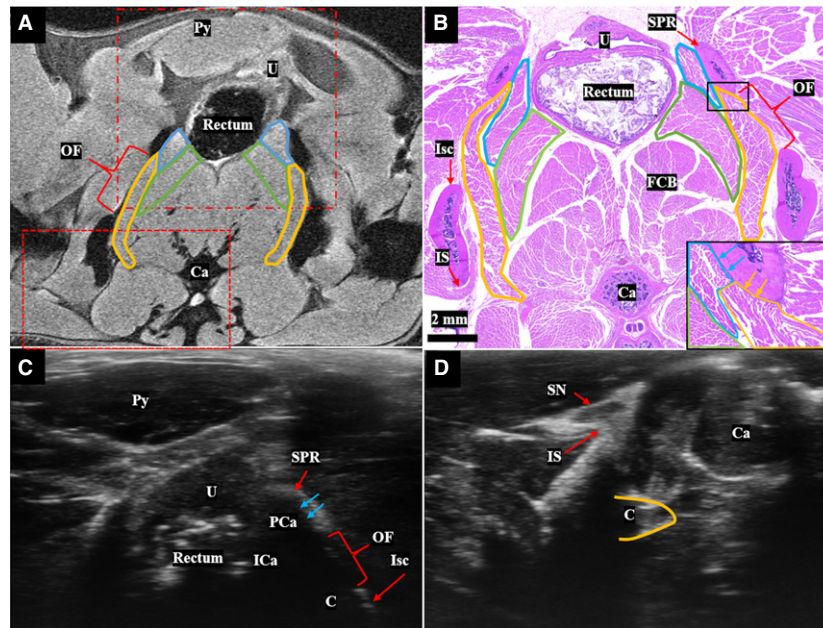


Fig. 3 (A) T2-weighted MR image at the level of the obturator foramen shows the origin of the pubocaudalis (blue outline) and coccygeus (yellow outline) at the medial superior pubic ramus. The body of iliocaudalis is shown in the green outline. This axial slice is slightly oblique so that the right side of the animal is more inferior than the left. The fields of view of the ultrasound images in (C) and (D) are shown by the dot/dash and dashed red boxes, respectively. (B) Cross-section at the level of the obturator foramen stained with hematoxylin and eosin, showing the origin of pubocaudalis (blue outline), iliocaudalis (green outline), and the origin of coccygeus (yellow outline). Inset image (black box) highlights origin of the coccygeus from the pubic bone. (C) The superior pubic ramus can be used as a bony landmark to identify the origin of the pubocaudalis on ultrasound. The approximate positions of iliocaudalis and coccygeus at this level are also shown. (D) Dorsal axial ultrasound view demonstrating the coccygeus (yellow outline) in the window between the ischial spine and the caudal vertebrae. Bl, Bladder; C, coccygeus; Ca, caudal vertebra; FCB, flexor caudalis brevis; ICa, iliocaudalis; IS, ischial spine; OF, obturator foramen; PCa, pubocaudalis; Py, pyramidalis muscle; SN, sciatic nerve; SPR, superior pubic ramus; U, uterus.

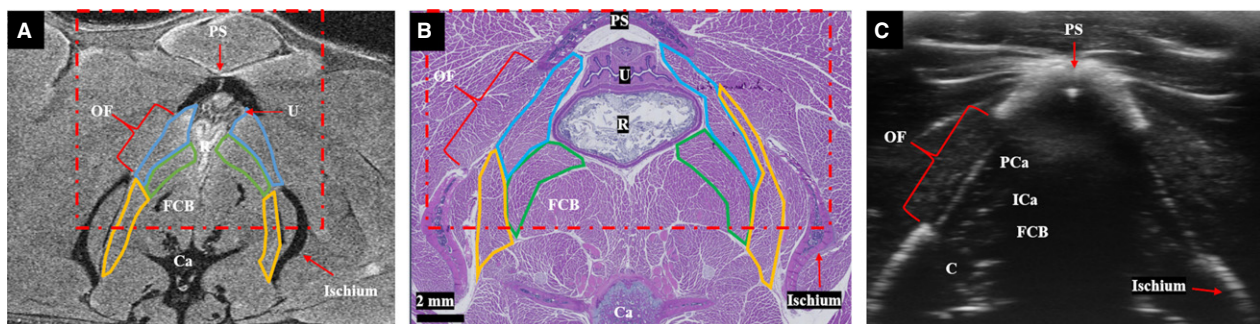


Fig. 4 (A) T2-weighted magnetic resonance image at the level of the pubic symphysis, demonstrating all three pelvic floor muscles, with pubocaudalis outlined in blue, iliocaudalis in green, and coccygeus in yellow. (B) Corresponding muscle histology at the level of the pubic symphysis. For (A) and (B), the red dot/dash box shows the field of view of the ultrasound (C) at the same level. (C) Axial ultrasound at the level of pubic symphysis. The obturator foramen provides a sonographic and anatomic window on the pelvic floor muscles. The intramuscular tendon of the iliocaudalis is visible as an echogenic focus. The central shadow is caused by the pubic symphysis. Bl, bladder; C, coccygeus; Ca, caudal vertebral body; FCB, flexor caudalis brevis; ICa, iliocaudalis; PCa, pubocaudalis; PS, pubic symphysis; Py, pyramidalis muscle; R, rectum; SN, sciatic nerve; U, uterus.

Table 1 Summary of imaging levels of interest with important landmarks.

Imaging level	Useful landmarks	Visible pelvic floor muscles	Associated figure
Sacroiliac	Sciatic nerve Flexor caudalis brevis and longus muscles	None	Fig. 2A
Acetabulum		Origin of iliocaudalis	Fig. 2B–D
Obturator Foramen	Superior pubic ramus	Origin of coccygeus Origin of pubocaudalis Body of iliocaudalis	Fig. 3
Pubic Symphysis	Obturator foramen	Bodies of coccygeus, iliocaudalis, and pubocaudalis	Fig. 4

important landmark, as the flexor caudalis brevis and flexor caudalis longus muscles, which could be mistaken for the pelvic floor muscles, can be easily identified at the sacroiliac level (Fig. 2A). Flexor caudalis brevis and flexor caudalis longus are a complex of muscle fascicles and long tendons arising from the lower lumbar, sacral, and proximal caudal vertebral bodies and inserting on the more distal caudal vertebrae (Brink & Pfaff, 1980). A second landmark for this level is the sciatic nerve, which originates from spinal segments L4–L6 and can be seen at the lateral margin of the flexor caudalis brevis muscle (Fig. 2A). In contrast, the sciatic nerve does not abut PFMs, which originate inferior to the sacroiliac level (Fig. 2B).

In cranial to caudal progression, the acetabulum is the next useful landmark. The acetabulum forms from the

triradiate cartilage, a Y-shaped structure with contributions from the ilium superiorly, pubis anteriorly, and ischium posteriorly. Iliocaudalis originates from the inferior medial surface and ventral border of the ilium, above the triradiate cartilage (Figs 1C and 2B). At this level, the body of the uterus and bladder can be seen anterior to the rectum. On axial ultrasound, the origin of iliocaudalis may be shadowed by the ilium and by stool in the rectum, if present (Fig. 2C). As one progresses from superior to inferior aspects of the acetabulum, the superior pubic ramus and a more ventrally located origin of pubocaudalis become visible on MRI and the corresponding two-dimensional histological cross-sectional images (Fig. 2B,D).

Below the level of the acetabulum, cranial and ventral to the obturator foramen, the origins of pubocaudalis and coccygeus from the superior pubic ramus are seen, with the latter more dorsally located (Fig. 3). At the obturator foramen level, the MR and histology images show the iliocaudalis muscle belly, located between pubocaudalis, flexor caudalis brevis, and coccygeus muscles (Fig. 3A,B). Pubocaudalis has a broad origin along the superior pubic ramus and courses inferiorly and lateral to iliocaudalis before inserting at the lateral aspect of the tail at the level of caudal vertebrae (Ca) Ca3 and Ca4. Coccygeus has a more horizontal and dorsal course towards its insertion on Ca1 and Ca2. Importantly, the ventral surface of the superior pubic ramus, visible on axial ultrasound image at this level, can be used as a landmark for the pubocaudalis origin (Fig. 3C). In the superior third of the obturator foramen, coccygeus covers the deep surface of the obturator foramen. From a posterior axial ultrasound view (Fig. 3D), coccygeus can be seen in the window between the ischial spine and Ca. The corresponding region as seen on MRI is illustrated in Fig. 3A.

At the level of the pubic symphysis, all three PFM bellies are visible, with pubocaudalis ventral and lateral, iliocaudalis more medial, and coccygeus dorsal and lateral

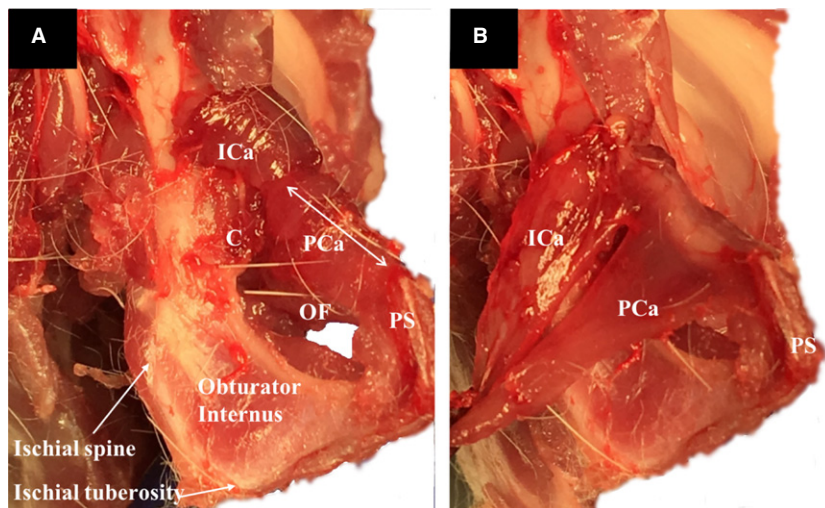


Fig. 5 (A) Medial view of the female rat left hemipelvis, demonstrating the origin of the coccygeus. The pubocaudalis and iliocaudalis reflected laterally over the superior pubic ramus to aid with visualization. (B) Gross anatomy of the origins of the pubocaudalis and iliocaudalis. The muscles had been detached at the insertion site. C, coccygeus; ICa, iliocaudalis; OF, obturator foramen; PCa, pubocaudalis; PS, pubic symphysis.

(Fig. 4A). Corresponding histology at this level (Fig. 4B) demonstrates the boundaries of PFMs to better advantage. The obturator foramen is the largest at this level, as shown on the MR (Fig. 4A) and ultrasound (Fig. 4C) images, providing an excellent sonographic window through which pubocaudalis, iliocaudalis, and coccygeus can be seen. A summary of the important levels and landmarks is provided in Table 1.

The gross anatomic relationships of the PFM origins are shown in Fig. 5 from a medial view of the left hemipelvis after disarticulation of the pubic symphysis. These anatomic dissections clearly show that the coccygeus arises from the pubis, with its origin located dorsal to that of pubocaudalis. The above arrangement differs from humans, in whom the coccygeus originates from the ischial spine. Also, in contradistinction to humans, the obturator internus muscle in the rat does not cover the obturator foramen but occupies the medial concave fossa of the ischium. In addition, the rat PFMs appear larger relative to the other muscles in the pelvis and have more distinct borders for the individual components of the PFM complex, compared with the analogous human PFMs (Fig. 6).

Once the anatomy and the relationship of the PFMs with respect to the surrounding pelvic structures were reliably

delineated using our multimodal approach, we went on to assess whether these muscles could be targeted using imaging guidance. To do this, we performed ultrasound-guided injections of a hydrogel laden with a fluorophore via a trans-obturator foramen approach (Fig. 7A). Successful injections were confirmed by the presence of hydrogel within PFMs, as demonstrated by fluorescent microscopic examination of muscle cross-sections (Fig. 7B).

Discussion

The need to elucidate the causes and pathogenesis of PFM dysfunction and related pelvic floor disorders is clear: until basic mechanisms are better understood, treatments will continue to be compensatory, offering marginal promise at best. The use of the cost-effective and less sentient rodent models is essential for bridging the existing large knowledge gaps. In addition, minimally invasive approaches for the delivery of novel preventative and therapeutic materials to the PFMs, located deep in the pelvis, are vital for the longitudinal preclinical studies with high translational potential. Furthermore, methods to evaluate the effects of such therapies on the PFM intrinsic components *in vivo* are equally important.

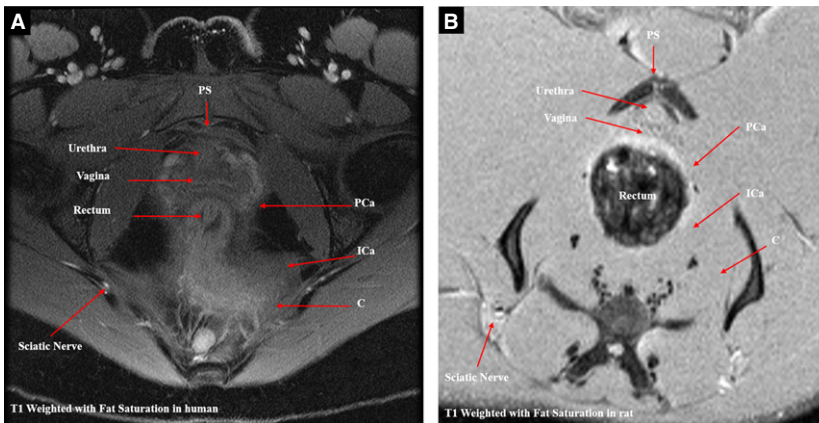


Fig. 6 Comparison of homologous pelvic floor muscles in the human and rat. (A) T1-weighted with fat saturation magnetic resonance image (MRI) of pelvic floor muscles at the level of pubic symphysis in a 30-year-old nulliparous premenopausal woman. (B) T1-weighted with fat saturation magnetic resonance image of rat female pelvic floor muscles at the level of pubic symphysis. C, coccygeus; ICa, iliococcygeus and iliocaudalis; PCa, pubcoccygeus and pubocaudalis in human and rat, respectively.

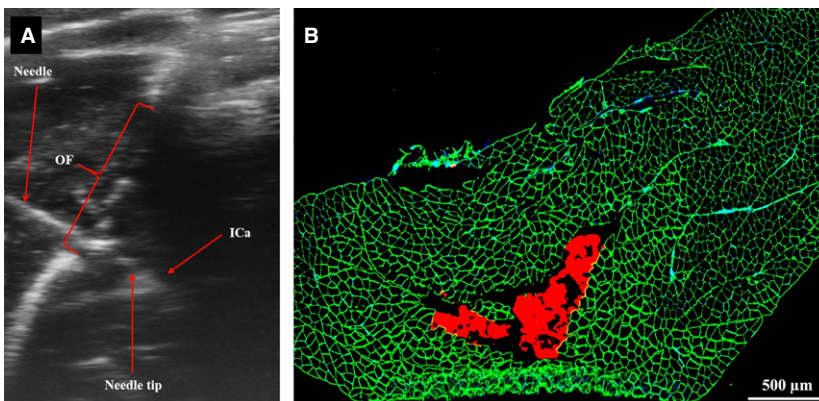


Fig. 7 (A) Ultrasound-guided injection of iliocaudalis muscle through the obturator foramen with hydrogel labeled with a red fluorophore. (B) Fluorescent microscopic image of the iliocaudalis cross-section, demonstrating successful injection of the hydrogel into the muscle belly (red). Muscle fibers demonstrated with the aid of laminin staining (green).

To achieve these goals, a detailed three-dimensional anatomy of the rat PFMs is required. The focus of the existing studies utilizing the radiological modalities has been on male rats or the pelvic viscera of both sexes (Suzuki et al. 1991). Published studies of the rat PFMs employ gross dissections to delineate muscle anatomy (Greene, 1935; Brink & Pfaff, 1980; Bremer et al. 2003; Thor & de Groat, 2010; Alperin et al. 2014). These investigations preclude longitudinal studies that assess PFM plasticity under variable physiological conditions, as well as muscle recovery following birth injury. In addition, these studies vary with respect to the origin of the coccygeus as either from the ischium (Thor & de Groat, 2010) vs. the pubis, deep or caudal to pubocaudalis (Brink & Pfaff, 1980; Bremer et al. 2003). To our knowledge, this is the first report of the radiographic appearance of female rat PFMs, delineated on MR and ultrasound imaging, coupled with the description of the PFM relationship to the major bony landmarks, identified by high-resolution micro CT, and validated by the two-dimensional histological analysis and gross anatomic dissections.

The three imaging modalities used in the current study have different strengths and weaknesses and can often be complementary (Bushberg, 2002). Briefly, ultrasound offers the chance to perform real time imaging for procedure guidance, as well as possible quantification of tissue properties, but is limited by dependence on operator experience, small depth of penetration, and lower soft tissue contrast. MRI offers whole field of view imaging with high soft tissue contrast but is more time-consuming and expensive compared to ultrasound, which impacts its feasibility. CT offers higher resolution and provides better delineation of osseous structures than MRI or ultrasound, but has more limited soft tissue contrast than MRI for evaluation of PFMs. The choice of a single method or a combination of various modalities should be guided by the specific research question at hand. For example, our multi-modality approach allowed us definitively to answer the question related to the origin of the rat coccygeus, confirming that this muscle arises from the pubic bone posterior to pubocaudalis (Figs 1C and 2D).

Delineating the normal imaging appearance of PFMs on MRI and ultrasound enables a systematic and accurate assessment of muscle changes in response to the increased mechanical load and unique hormonal milieu associated with pregnancy, spontaneous delivery, simulated birth, and postpartum regeneration in the longitudinal *in vivo* rat model. The rapidly increasing quantitative capabilities of ultrasound and MRI have a high potential for noninvasive assessments of the structural and functional properties of PFM, such as fiber length, fibrotic and fatty muscle infiltration, and muscle stiffness, in the near future (Fielding et al. 2000; Constantinou, 2009; Damon et al. 2011; Zaidman et al. 2011; Hakim et al. 2015). Once such changes are delineated in the animal model, a subset of these parameters can be explored in women using non-invasive imaging

modalities. The above will enable the development of high-resolution tools for diagnostic or prognostic applications. For example, correlating the extent of changes prior to delivery with postpartum outcomes can potentially identify women at high risk for PFM injury and provide clinicians with objective criteria on which to base individualized patient counselling regarding the mode of delivery. In addition, a detailed understanding of PFM anatomy enables the use of ultrasound to guide minimally invasive percutaneous techniques for the delivery of local therapies for injured PFMs. In this study, we demonstrated that all three PFMs can be successfully targeted through the obturator foramen (Figs 3C, 4B, and 7). Alternately, the coccygeus muscle could also be targeted via a posterior approach.

Acknowledgements

Dr. Sheth received support from the UCSD Clinician Scientist Radiology Resident Program and NIBIB T32-EB005970. The project described was partially supported by funds provided by the National Institutes of Health Grant UL1TR001442 of CTSA and by funds provided by the University of California, San Diego (UCSD) Chancellor. The content is solely the responsibility of the authors and does not necessarily represent the official views of the NIH. The authors have no conflicts of interest to disclose.

Author contributions

V.S.: study design, data acquisition and interpretation, manuscript writing. P.D.: data acquisition, manuscript writing. J.W.: data acquisition. S.S.: concept and study design, manuscript writing. J.D.: data acquisition and processing. K.C.: manuscript writing and editing. E.C.: concept and study design; data acquisition and interpretation, manuscript writing. M.A.: concept and study design, data acquisition and interpretation, manuscript writing and editing.

Funding

NIH/NICHD R01HD092515 (M.A.); NIH/NICHD R21HD094566 (M.A., K.L.C.); NIH UL1TR001442; NIH/NIA R03AG050951 (M.A.).

References

- Alperin M, Feola A, Meyn L, et al. (2010) Collagen scaffold: a treatment for simulated maternal birth injury in the rat model. *Am J Obstet Gynecol* **202**, 589 e581–588
- Alperin M, Tuttle LJ, Conner BR, et al. (2014) Comparison of pelvic muscle architecture between humans and commonly used laboratory species. *Int Urogynecol J* **25**, 1507–1515.
- Alperin M, Lawley DM, Esparza MC, et al. (2015) Pregnancy-induced adaptations in the intrinsic structure of rat pelvic floor muscles. *Am J Obstet Gynecol* **213**, 191 e191–197.
- Alperin M, Kaddis T, Pichika R, et al. (2016) Pregnancy-induced adaptations in intramuscular extracellular matrix of rat pelvic floor muscles. *Am J Obstet Gynecol* **215**, 210 e211–217.

- Bremer RE, Barber MD, Coates KW, et al.** (2003) Innervation of the levator ani and coccygeus muscles of the female rat. *Anat Rec A Discov Mol Cell Evol Biol* **275**, 1031–1041.
- Brink EE, Pfaff DW** (1980) Vertebral muscles of the back and tail of the albino rat (*Rattus norvegicus albinus*). *Brain Behav Evol* **17**, 1–47.
- Bushberg JT** (2002) *The Essential Physics of Medical Imaging*. Philadelphia: Lippincott Williams & Wilkins.
- Catanzarite T, Bremner S, Barlow CL, et al.** (2018) Pelvic muscles' mechanical response to strains in the absence and presence of pregnancy-induced adaptations in a rat model. *Am J Obstet Gynecol* **218**, 512. e1–e9.
- Constantinou CE** (2009) Dynamics of female pelvic floor function using urodynamics, ultrasound and magnetic resonance imaging (MRI). *Eur J Obstet Gynecol Reprod Biol* **144**, S159–S165.
- Cruz M, Dissaranan C, Coteleur A, et al.** (2012) Pelvic organ distribution of mesenchymal stem cells injected intravenously after simulated childbirth injury in female rats. *Obstet Gynecol Int* **2012**, 612946.
- Damon BM, Buck AKW, Ding Z** (2011) Diffusion-tensor MRI based skeletal muscle fiber tracking. *Imaging Med* **3**, 675–687.
- Feola A, Endo M, Deprest J** (2014) Biomechanics of the rat vagina during pregnancy and postpartum: a 3-dimensional ultrasound approach. *Int Urogynecol J* **25**, 915–920.
- Fielding JR, Dumanli H, Schreyer AG, et al.** (2000) MR-based three-dimensional modeling of the normal pelvic floor in women: quantification of muscle mass. *AJR Am J Roentgenol* **174**, 657–660.
- García del Salto L, de Miguel Criado J, Aguilera del Hoyo LF, et al.** (2014) MR imaging-based assessment of the female pelvic floor. *Radiographics* **34**, 1417–1439.
- Greene EC** (1935) *Anatomy of the Rat, Transactions of the American Philosophical Society*. New York: Hafner.
- Hakim L, Endo M, Feola A, et al.** (2015) High-frequency micro-ultrasound: a novel method to assess external urethral sphincter function in rats following simulated birth injury. *Neurourol Urodyn* **34**, 264–269.
- Handa VL, Blomquist J, Knoepp L, et al.** (2011) Pelvic floor disorders 5–10 years after vaginal or cesarean childbirth. *Obstet Gynecol* **118**, 777–784.
- Lukacz E, Lawrence J, Contreras R, et al.** (2006) Parity, mode of delivery, and pelvic floor disorders. *Obstet Gynecol* **107**, 1253–1260.
- Memon HU, Handa VL** (2013) Vaginal childbirth and pelvic floor disorders. *Womens Health (Lond)* **9**, 265–277; quiz 276–267.
- Meng H, Janssen PM, Grange RW, et al.** (2014) Tissue triage and freezing for models of skeletal muscle disease. *J Vis Exp* **15**, 89.
- Peel JH** (1949) Discussion on the role of physiotherapy in the prevention and treatment of post-natal disorders. *Proc R Sci Med* **43**, 741–745.
- Peng Y, Miller BD, Boone TB, et al.** (2018) Modern theories of Pelvic floor support: a topical review of modern studies on structural and functional pelvic floor support from medical imaging, computational modeling, and electromyographic perspectives. *Curr Urol Rep* **19**, 9.
- Porter NH** (1960) A physiological study of the pelvic floor in rectal prolapse. *R Coll Surg Engl* **31**, 379–404.
- Stewart AM, Cook MS, Esparza MC, et al.** (2017) Architectural assessment of rhesus macaque pelvic floor muscles: comparison for use as a human model. *Int Urogynecol J* **28**, 1527–1535.
- Suzuki T, Takezawa Y, Tamura Y, et al.** (1991) Sectional anatomy of the pelvis in the male rat with ultrasound correlations. *Anat Rec* **231**, 275–285.
- Thor KB, de Groat WC** (2010) Neural control of the female urethral and anal rhabdosphincters and pelvic floor muscles. *Am J Physiol Regul Integr Comp Physiol* **299**, R416–R438.
- Wood H, Kuang M, Woo L, et al.** (2008) Cytokine expression after vaginal distention of different durations in virgin Sprague-Dawley rats. *J Urol* **180**, 753–759.
- Wu JM, Vaughan CP, Goode PS, et al.** (2014) Prevalence and trends of symptomatic pelvic floor disorders in U.S. women. *Obstet Gynecol* **123**, 141–148.
- Zaidman CM, Malkus EC, Siener C, et al.** (2011) Qualitative and quantitative skeletal muscle ultrasound in late-onset acid maltase deficiency. *Muscle Nerve* **44**, 418–423.